Chapter 10

Semiconductor Materials by Ultrasonic Spray Pyrolysis and Their Application in Electronic Devices

Miguel Dominguez, Jose A. Luna-Lopez and Francisco J. Flores

Additional information is available at the end of the chapter

http://dx.doi.org/10.5772/67548

Abstract

Ultrasonic spray pyrolysis is a deposition technique that enables a fine mist of the precursor solution in order to deposit higher-density thin films. This characteristic makes of great potential the use of ultrasonically spray-deposited semiconductors films for low-cost, transparent, flexible and large-area applications. In this chapter, low-temperature deposition and characterization of ultrasonically spray-deposited zinc oxide (ZnO) films are presented. The ZnO films deposited by ultrasonic spray pyrolysis at 200°C were characterized by optical transmittance, photoluminescence spectroscopy, X-ray diffraction and Fourier transform infrared spectroscopy. The study of low-temperature annealing of ZnO films is also presented. Moreover, the characterization of aluminum-doped ZnO films deposited by ultrasonic spray pyrolysis at 200°C is presented. Finally, applications of these ultrasonic spray-deposited films in electronic devices are presented.

Keywords: spray pyrolysis, low temperature, electronic devices

1. Introduction

Currently, semiconductor thin films are attractive to enable novel electronic applications. Deposition techniques such as pulsed laser deposition, chemical vapor deposition and sputtering have been used [1–4]. However, these deposition techniques present technical limitations such as low compatibility with large-area substrates, high cost and need of high or ultra-high vacuum. On the other hand, solution process techniques offer a solution to these problems at low cost and the possibility to deposit films under air ambient [5, 6]. The conventional solution-processed thin films by spin-coating have a low density due to pores during the annealing of the films [7]. However, ultrasonic spray pyrolysis is a deposition technique

that enables a fine mist of the precursor solution in order to deposit higher-density thin films. This characteristic makes of great potential the use of ultrasonic spray-deposited semiconductors films for low-cost, transparent, flexible and large-area applications.

Metal-oxide semiconductors are promising materials to be used in novel electronic applications. Applications, such as thin-film transistors (TFTs), sensors, electronic circuits, among others, have been reported [8–10]. The results reported by other authors show that the main limitation is the need to use high deposition temperatures to achieve high-quality semiconductor films, since low-temperature deposition may lead to an incomplete pyrolysis of the precursor solutions [11].

In this chapter, low-temperature deposition and characterization of ultrasonic spray-deposited zinc oxide (ZnO) films are presented. The ZnO films deposited by ultrasonic spray pyrolysis at 200°C were characterized by optical transmittance, photoluminescence (PL) spectroscopy, X-ray diffraction (XRD) and Fourier transform infrared (FTIR) spectroscopy. The study of low-temperature annealing of ZnO films is also presented. Moreover, the characterization of aluminum-doped ZnO films deposited by ultrasonic spray pyrolysis at 200°C is presented. Finally, applications of these ultrasonic spray-deposited films in electronic devices are presented.

2. Zinc oxide films deposited by ultrasonic spray pyrolysis at 200°C

Previous reports [11] show a dependency of the zinc oxide structure with deposition temperature. The crystallinity of the film is increased as the deposition temperature is higher. **Figure 1** shows the XRD pattern of the as-deposited ZnO film at 200°C. The pattern shows three-weak peaks at 2θ = 31.72°, 34.42° and 56.64°, which are associated with the (100), (002) and (110) planes, respectively. From the overall XRD diffractogram, the ZnO film tends to present some polycrystallinity and agree with the JCPDS Card No. 36-1451.

Figure 2 shows the optical transmittance of as-deposited ZnO films. It can be seen the highly transparent in the visible range of the film. The gap energy is extracted by the extrapolation of the linear region in the $(\alpha h\nu)^2 \sim A(h\nu\text{-}Eg)$ characteristics, where hν is the photon energy, α is the absorption coefficient, Eg is the gap energy and A is the constant. The extracted gap energy was 3.26 eV, which is similar than the commonly reported [5].

Figure 3 shows the FTIR spectra of the ZnO film. It can be observed the peak at 415 cm^{-1} related to Zn—O stretching modes [11, 12]. The peak at 1627 cm^{-1} is attributed to O—H bending modes. Also, the peaks at 2500–3500 cm^{-1} are due to C—H and O—H stretching modes [11, 12]. The peaks at 1413 cm^{-1} and 1530 cm^{-1} are attributed to C—O stretching modes, while at 1750 cm^{-1} to C═O bonds [11, 12]. The presence of C—O bonds suggests an incomplete precursor pyrolysis due to the low deposition temperature [11]. However, the characteristic Zn—O band approximately at 415 cm^{-1} indicates the ZnO formation. On the other hand, it is important to mention that bonds related to O—H stretching have been previously reported in ZnO films, indicating the presence of O—H complexes that are associated with different defects and increased free-carrier concentration [11–14].

http://dx.doi.org/10.5772/67548

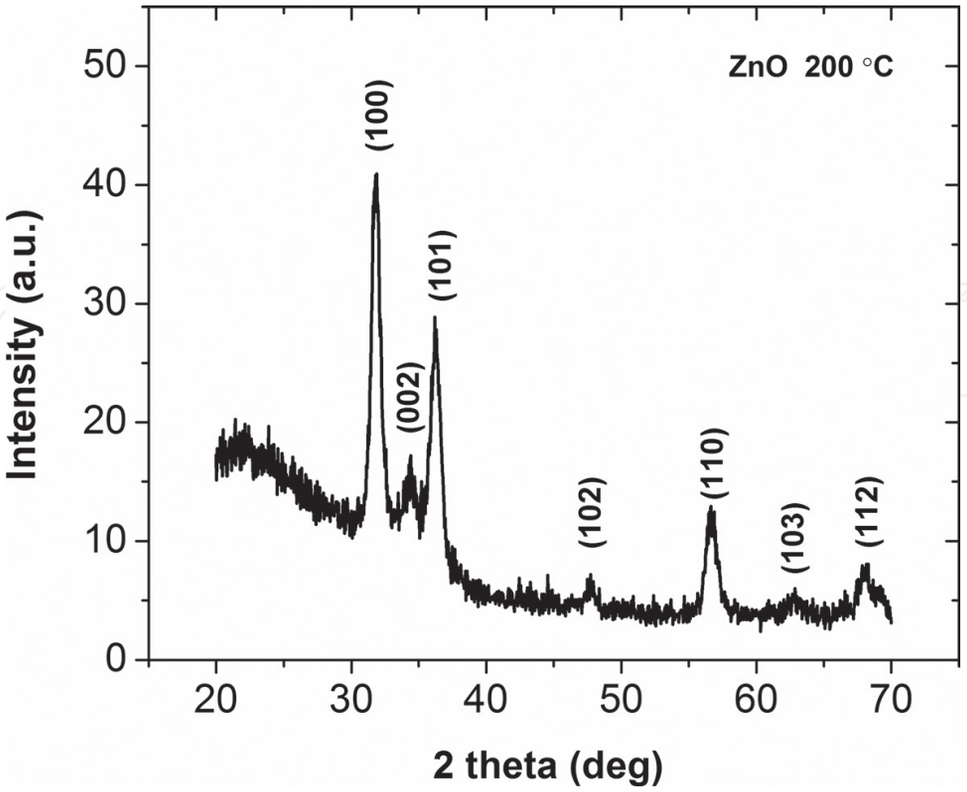

Figure 1. XRD pattern of the as-deposited ZnO films by ultrasonic spray pyrolysis.

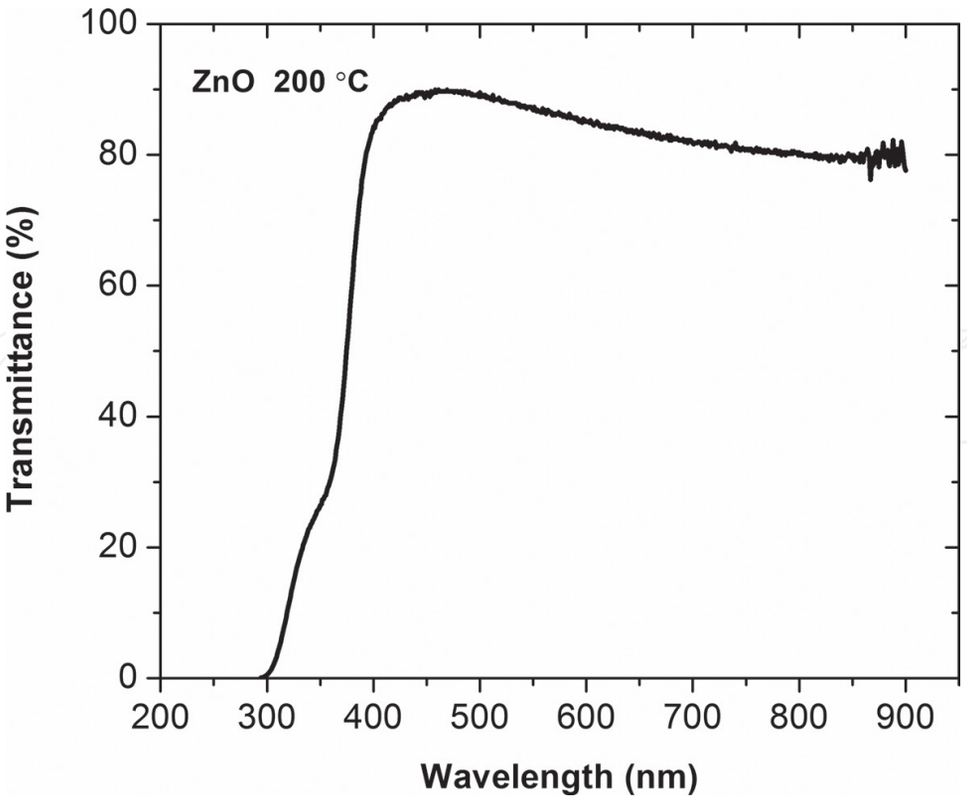

Figure 2. Transmittance of the as-deposited ZnO films by ultrasonic spray pyrolysis.

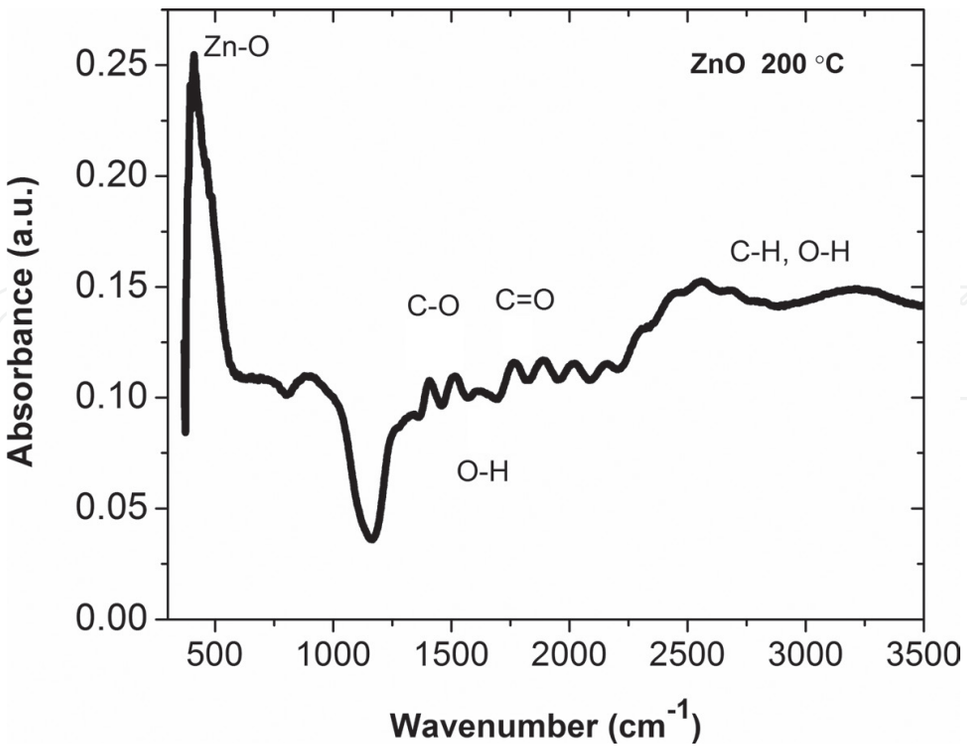

Figure 3. FTIR spectra of the as-deposited ZnO films by ultrasonic spray pyrolysis.

Figure 4 shows the photoluminescence (PL) spectra of the as-deposited ZnO film. It exhibits a PL spectrum with a peak centered at 390 nm of high intensity and a broad band from 450 to 700 nm. The peak at 390 nm (UV emission) is typically associated with the near band-edge (NBE) emission of the gap, which is attributed to the recombination of the free excitons [15, 16]. The broad band from 450 to 700 nm (visible emission) is typically associated with the impurities and defects, which are considerable in our case. The origin of this visible emission band has been related to zinc and oxygen vacancies, zinc and oxygen antisites, and to zinc and oxygen interstitials [16, 17]. Several authors have reported the use of photoluminescence spectroscopy to study the role of the defects and impurities in ZnO. However, even with the same experimental conditions they have reported contradictory results [17]. Therefore, since the impurities and defects are highly dependent on the deposition technique and its conditions, their role in the electronic properties of ZnO is still controversial.

2.1. Thermal annealing effects

The use of metal-oxide semiconductors in semiconductor devices is constantly increased, since thin-film transistors, solar cells, optical sensors, among others. In these devices, a high-quality metal-semiconductor interface is desired in order to avoid voltage drops which result in loss of performance. Ideally, a metal-semiconductor contact no exhibit barriers for the carrier flow in whatever polarization (positive or negative). This is true when there are no interface states, and the metal and semiconductor work functions are similar. However, obtaining

http://dx.doi.org/10.5772/67548

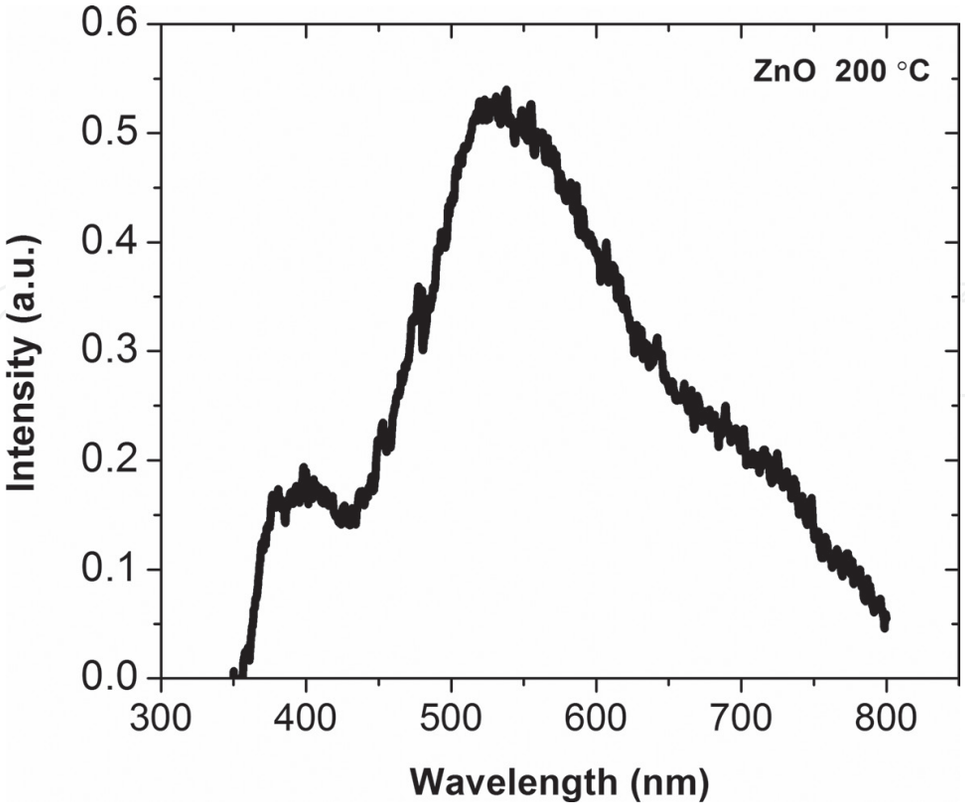

Figure 4. Photoluminescence of the as-deposited ZnO films by ultrasonic spray pyrolysis.

a metal-semiconductor contact without interface states is difficult. Moreover, matching the metal and semiconductor work functions is nearly impossible. It is well known that metal-oxide films are highly dependent on the deposition and post-treatments conditions, resulting in different surface conditions and defect density distribution. For this reason, different results have been reported.

Figure 5 shows the conductivity and contact resistance of Al-ZnO contacts annealed at 180°C as a function of annealing time. It exhibits a reduction of more than two orders of magnitude in contact resistance in samples annealed for 30 min. This improvement can be associated with a higher carrier injection through the Al-ZnO (metal-semiconductor) interface. Nunes et al. [6, 18, 19] reported that this is due to desorption of oxygen present at the grain boundaries. As result of this oxygen loss, there is an increase in the effective carrier concentration near to the Al-ZnO interface.

Also, an increase in the contact resistance with longer annealing time than 30 min is appreciated in **Figure 5**. This increase can be associated with a change in the ZnO film quality, as the reduction in conductivity shows. One can conclude that there is an optimal annealing time and after this time, the metal-semiconductor interface deteriorates. Using FTIR spectroscopy and XRD, the effects of the low temperature annealing on the ZnO film can be studied.

Figure 6 shows the FTIR spectra of ZnO films at different annealing times. The peak at 415 cm^{-1} was previously related to Zn—O stretching modes. The characteristic Zn—O peak

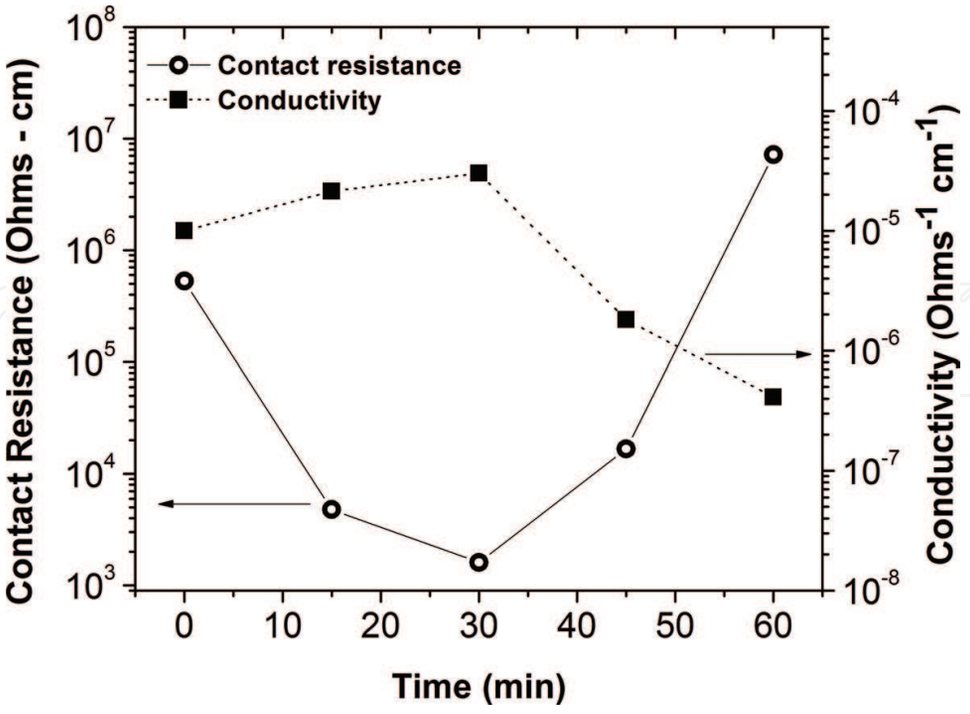

Figure 5. Al-ZnO contact resistance and conductivity extracted by TLM as a function of annealing time.

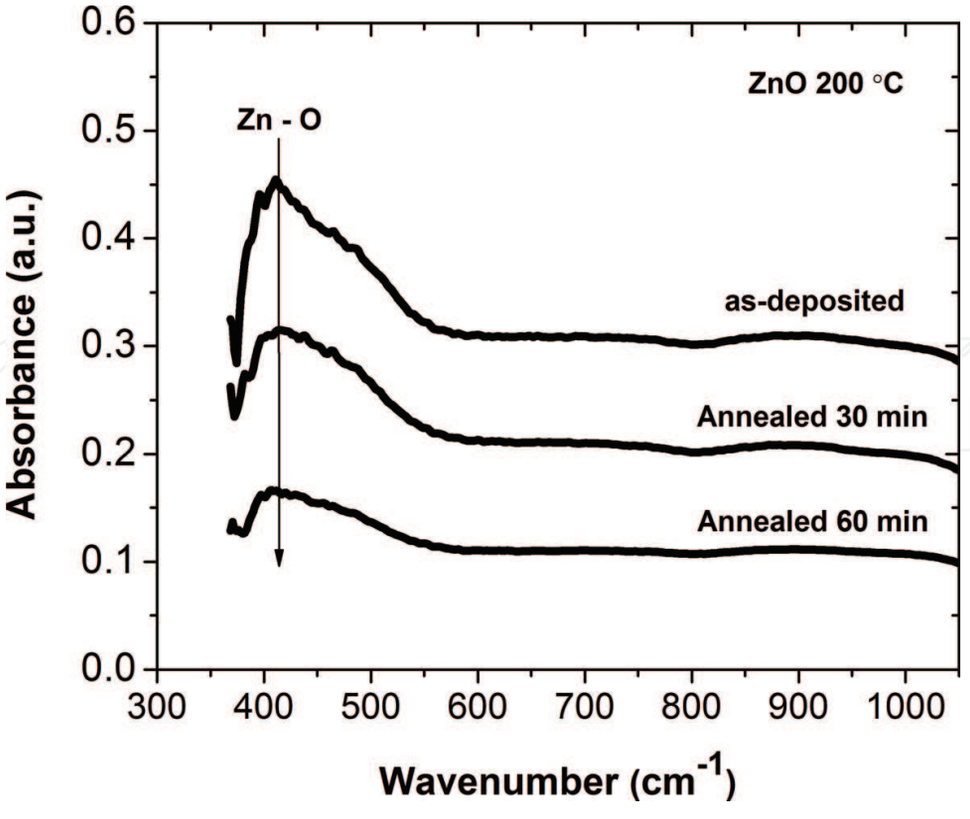

Figure 6. FTIR spectra of as-deposited and annealed ZnO films.

http://dx.doi.org/10.5772/67548

indicates the ZnO formation. A reduction in Zn—O bonds is clearly exhibited as the annealing time is increased. This agrees with the results of contact resistance and conductivity, where the carrier concentration is increased by oxygen vacancies. However, the progressive reduction in Zn—O bonds at 60 min of annealing may not explain the increase in contact resistance. In this case, **Figure 7** shows the XRD patterns of as-deposited and annealed ZnO films. In the as-deposited ZnO films, a strong peak associated with the (100) plane can be appreciated, and also peaks related to the planes (002), (101) and (110) can be identified. At 30 min of annealing, the strongest peak is now associated with the (002) plane. Also, peaks related to the planes (100), (101), (102), (103), (112) and (110) can be identified (in agreement with the JCPDS Card No. 36-1451). A better polycrystalline nature of ZnO films for 30 min of annealing can be confirmed. The preferential orientation in (002) plane has been reported in high-quality ZnO films [11, 20]. Finally, at 60 min of annealing, the preferential orientation in (002) plane disappeared and also the peaks related to the planes (102) and (103). A reduction in the peaks related to the planes (100) and (101) is appreciated. The FTIR spectroscopy and XRD results confirm the degradation of the ZnO film after 60 min of annealing and agree with the contact resistance and conductivity results.

2.2. Aluminum-doped zinc oxide films

Typically, the zinc oxide film is doped with different impurities such as aluminum (Al), cadmium or gallium in order to increase its conductivity. In this case, aluminum was used as a doping source. **Figure 8** shows the optical transmittance of the AZO films at different

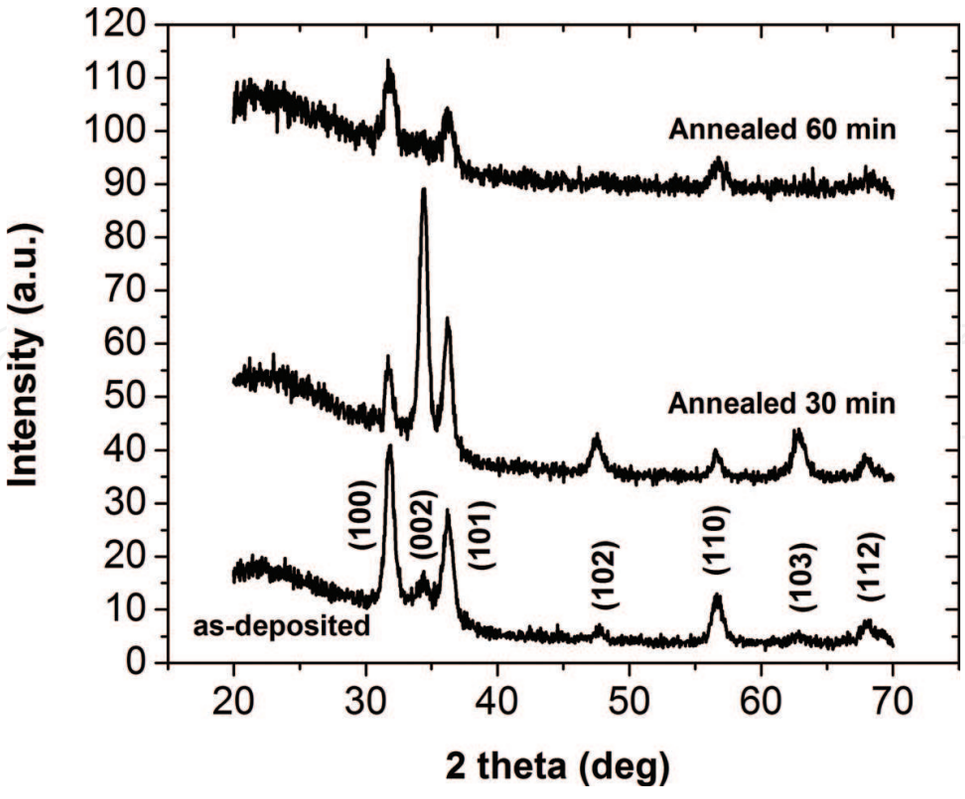

Figure 7. XRD patterns of as-deposited and annealed ZnO films.

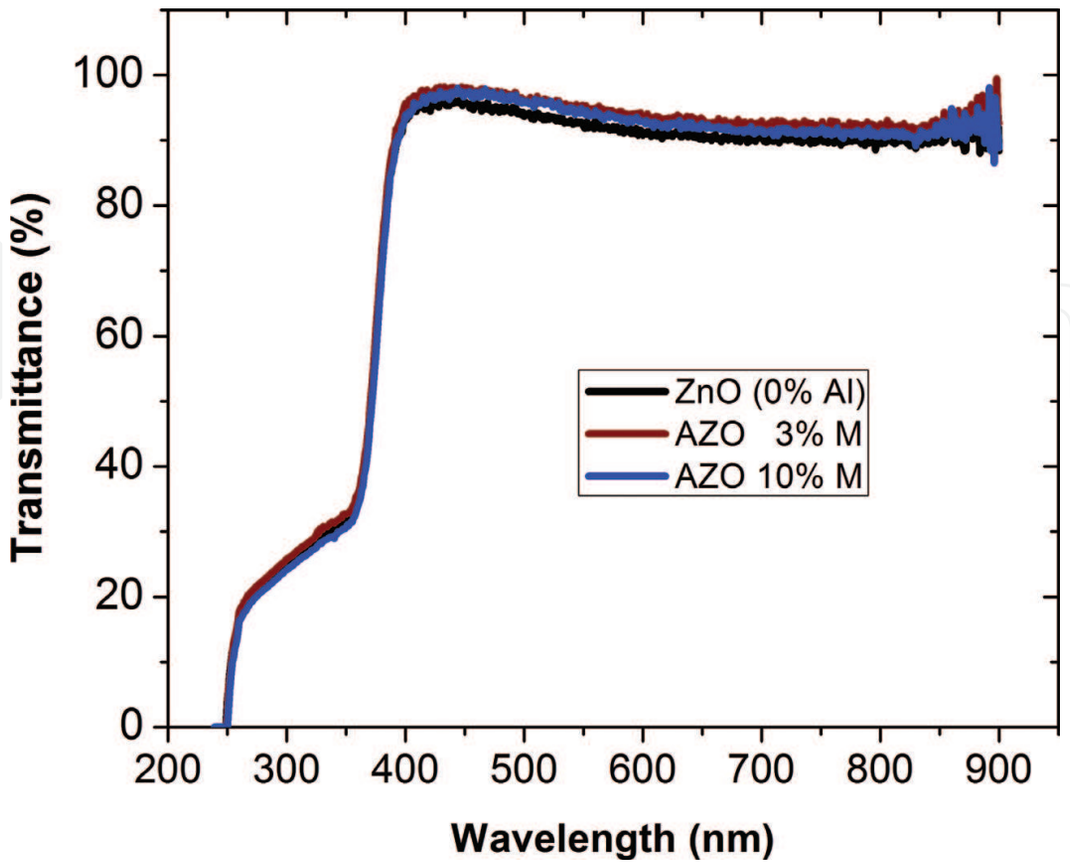

Figure 8. Optical transmittance of the AZO films at different aluminum-doping concentrations.

aluminum-doping concentrations. The films are highly transparent in the visible range. It is important to note that the increase in the doping concentration has no effect on the optical transmittance. This agrees with the reported information in Ref. [20].

Figure 9 shows the XRD pattern of the AZO films at different aluminum-doping concentrations. The AZO films show an amorphous structure regardless of the Al-doping concentration, since no presence of peaks is exhibited. This is expected due to the low temperature of deposition [11].

Figure 10 shows the resistivity of the AZO films at different aluminum-doping concentrations. It can be observed that the resistivity decreases as the doping concentration increases at 3 M%. This decrease in resistivity is considered as result of the increase in carrier concentration. The increase in carrier concentration of AZO films is due to the substitutional incorporation of Al^{3+} ions at Zn^{2+} cation sites or the incorporation of Al ions in interstitial positions [21]. However, as the doping concentration increases above 3 M%, the AZO resistivity also increases. This increase in resistivity is attributed to a decrease in the mobility of carriers resulted by ionized impurity scattering [22]. This agrees with that reported by other authors [21, 23], where the excessive Al-doping deteriorates the properties of the AZO films due to the formation of stress by the smaller radius of Al^{3+} ions compared with Zn^{2+} ions.

http://dx.doi.org/10.5772/67548

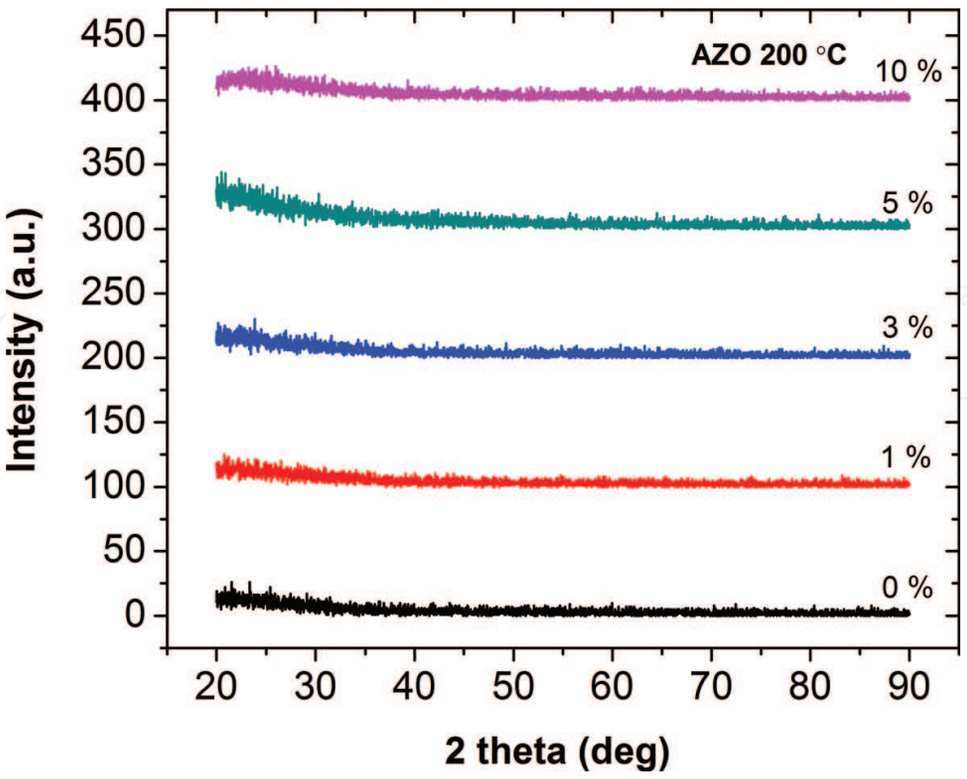

Figure 9. XRD patterns of the AZO films at different aluminum-doping concentrations.

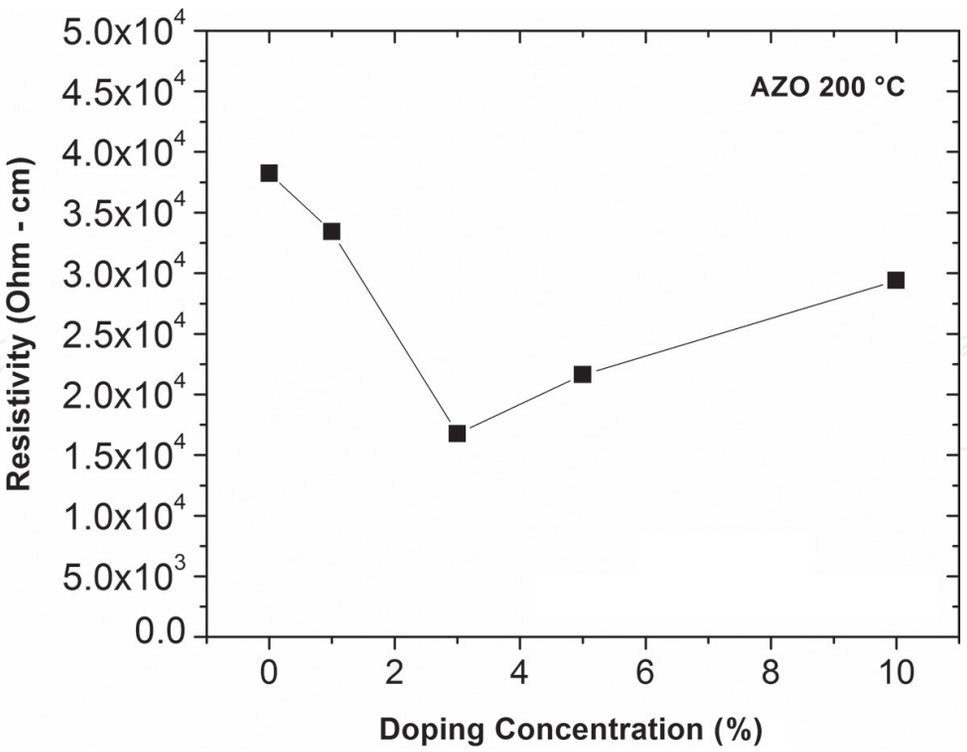

Figure 10. Resistivity of the AZO films at different aluminum-doping concentrations.

3. Applications in electronic devices

An important area of the materials science is the application of the materials obtained. The advantages of spray pyrolysis make of great potential the use of semiconductors as active layers in electronic devices. In recent years, the development of low-cost electronics has achieved a considerable progress, since wearable electronics, transparent circuitry, e-paper, solar cells and more.

3.1. Fully solution-processed transparent MIS capacitors

This basic device can work as energy storage from solar cells, sensor, memory device and charge-discharge capacitor in active-matrix displays and also can be very useful to analyze the quality of the dielectric-semiconductor interface in field-effect devices. In this section, we present fully solution-processed capacitors employing the ultrasonic spray pyrolysis and spin-coating techniques. Zinc oxide films deposited by ultrasonic spray pyrolysis were used as an active layer and spin-on glass (SOG) is used as dielectric. The maximum fabrication temperature used was set at 200°C. **Figure 11** shows a top-view photograph of the MIS capacitors. The MIS capacitors are highly transparent, which is used in transparent electronics.

Figure 12 shows the capacitance-voltage characteristics at 10 KHz for the MIS capacitors. When a negative voltage is applied at the top contact, there is an accumulation layer of electrons in the ZnO film at the SOG/DI-ZnO (dielectric-semiconductor) interface; as a result, the capacitance-voltage characteristics exhibit the dielectric capacitance (C_{ox}). On the other hand, when a positive voltage is applied at the top contact, there is a depletion region in the ZnO film at the SOG/DI-ZnO interface; then, the capacitance-voltage characteristics show a

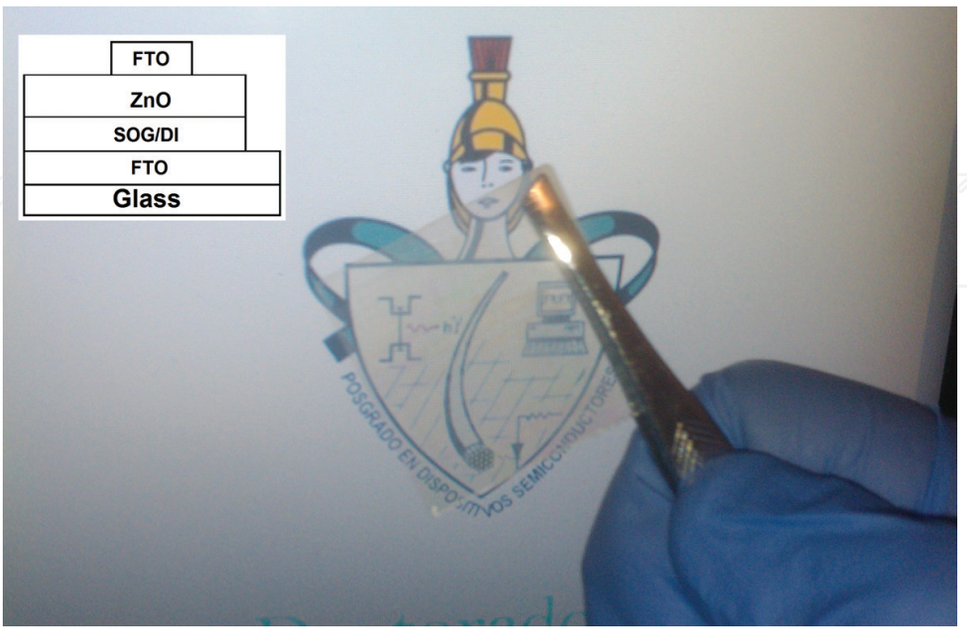

Figure 11. Top-view photograph of the MIS capacitors.

http://dx.doi.org/10.5772/67548

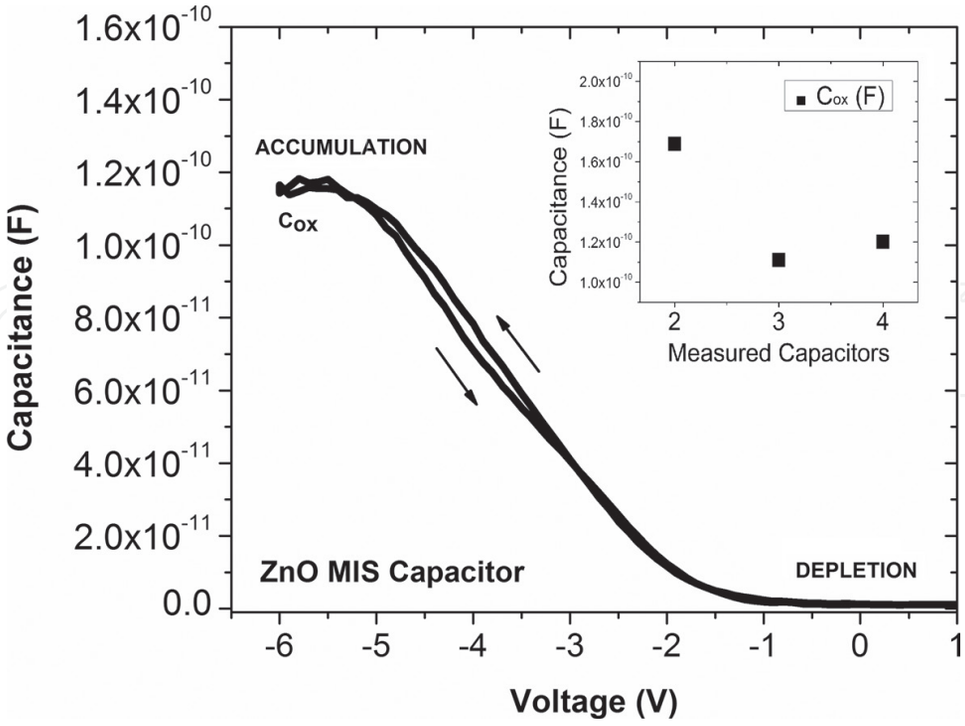

Figure 12. Forward and reverse capacitance-voltage curves of the ZnO MIS capacitors.

minimum capacitance. The capacitance-voltage measurements exhibit a very low hysteresis when the characteristics are forward and reverse measured. However, at negative voltage values, the accumulation region presents effects of interface states [24]. This is attributed to the defects in the ZnO film near at the dielectric-semiconductor interface, as the photoluminescence and FTIR spectroscopies show.

On the other hand, **Figure 13** shows the current density of the ZnO MIS capacitors. The breakdown voltage of the MIS capacitor can be appreciated at 36 V, which is due to the dielectric breakdown. The values of current density and capacitor breakdown voltage obtained are reliable for electronic device applications [25, 26].

The ZnO MIS capacitors were fabricated employing simple and low-cost solution process techniques with no-vacuum need, using feasible and easily prepared precursor solutions.

3.2. Flexible metal-insulator-semiconductor diodes

The semiconductor diodes are known as devices that allow the flow of current in only one voltage bias (positive or negative). These devices are extensively used in electronics such as circuit protection, rectifiers, mixing, isolating and detection signals. Recently, Son et al. [27] reported for the first time Schottky diodes using solution-processed zinc tin oxide on corning glass. Alternatively to PN and Schottky diodes, metal-insulator-semiconductor (MIS) diodes are devices, which used a thin insulator film, that allow the tunneling of carriers in only one voltage bias. For this reason, these devices are also known as MIS tunnel diodes [28–31]. Güllü et al. [32] reported the application of MIS diodes as temperature sensors.

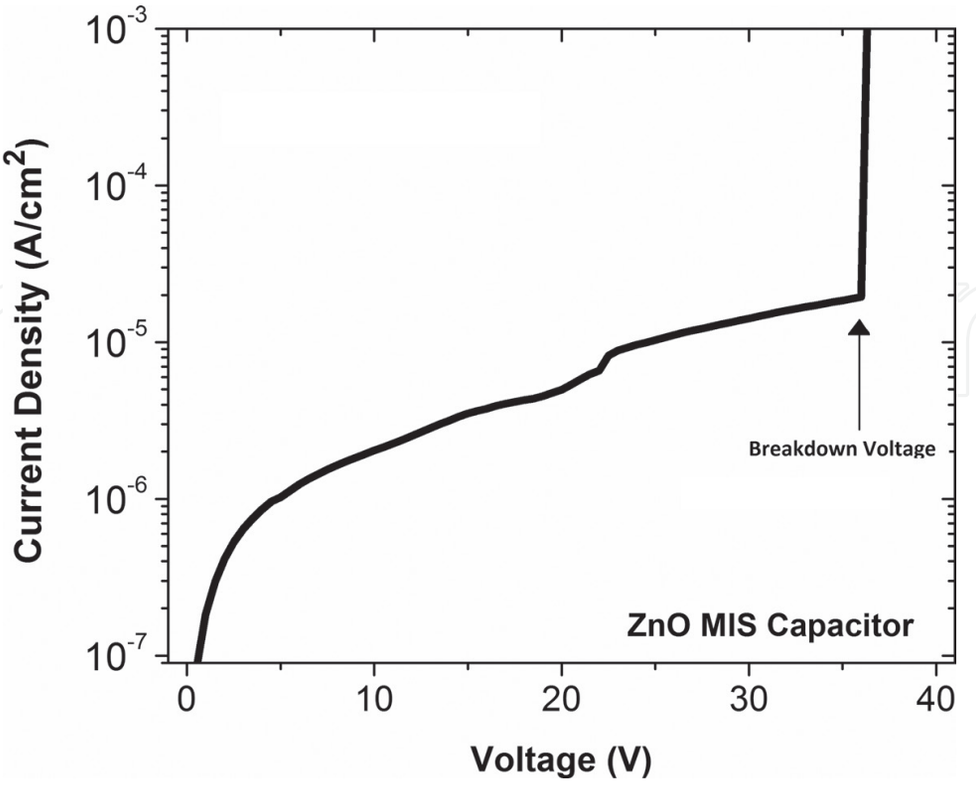

Figure 13. Current density of the ZnO MIS capacitors.

In this section, the fabrication and characterization of fully solution-processed flexible metal-insulator-semiconductor diodes is presented. As an active layer, aluminum-doped zinc oxide (AZO) thin film by ultrasonic spray pyrolysis was used. As an insulator, a silicon oxide thin film by spin-on glass (SOG/DI) was used. The maximum temperature used was 200°C. As far as the authors know, this is the first flexible solution-processed MIS diode using amorphous oxide semiconductors.

To fabricate the flexible MIS diodes, the AZO film with Al-doping concentration at 3 M% was used, which exhibits the best doping efficiency.

Figure 14 shows the electrical characteristics of the flexible MIS diodes. A good rectifying behavior is observed when negative voltage is applied to the ITO contact (reverse bias), and the current is independent of the voltage applied. When a positive voltage is applied to the ITO contact (forward bias), the injected carriers are collected by tunneling through the insulator; then, the current increases exponentially with increasing bias. The inset in **Figure 14** shows the inverse saturation current, which is close to 150 pA. An on/off current ratio of 10^2 is reached at |4|V. This value is similar to other diodes reported by other authors at higher fabrication temperature [27, 31]. The forward bias current in a MIS diode is assumed to be due to thermionic emission and can be expressed as [32]:

$$I = I_0 \exp\left(qV/nkT\right) \tag{1}$$

http://dx.doi.org/10.5772/67548

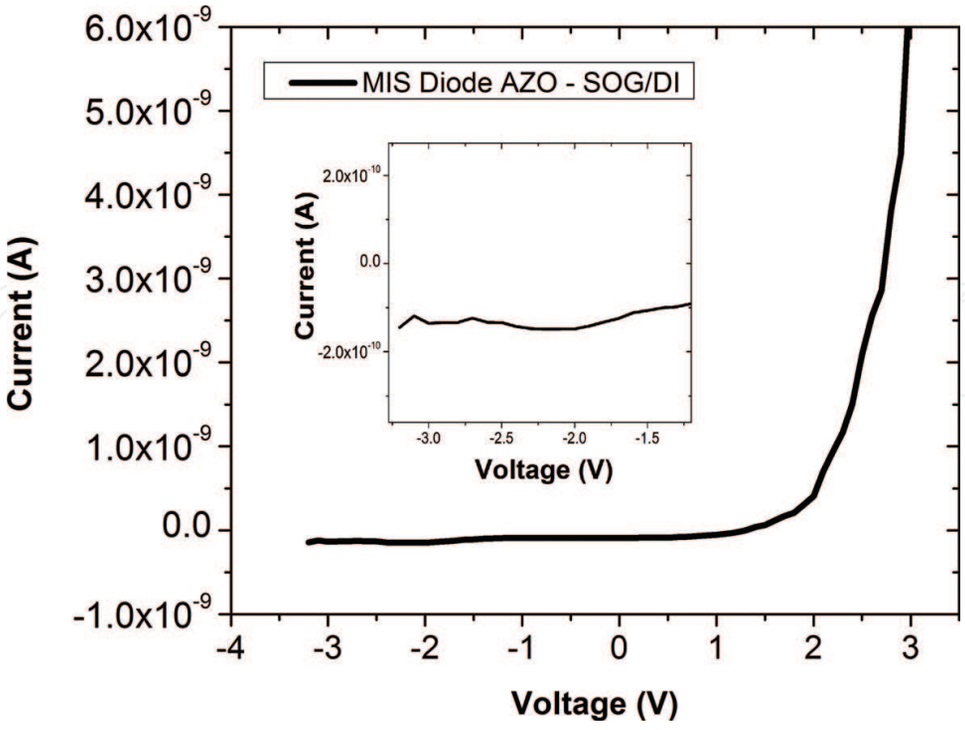

Figure 14. Electrical characteristics of the flexible MIS diodes. Inset: inverse saturation current.

where I_0 is the saturation current, q is the electron charge, *n* is the ideality factor, *k* is the Boltzmann constant and T is the temperature in K. The saturation current I_0 can be expressed as:

$$I_0 = AA^* T^2 \exp\left(-q\Phi_B / kT\right) \tag{2}$$

where A is the diode area, A^* is the effective Richardson constant of 32 A/cm^{2}K^2 for ZnO [33], and Φ_B is the barrier height.

Typically, the ideality factor and barrier height can be extracted from the extrapolation to 0 V and its slope of the linear region of the forward bias of ln(I)-V characteristics [30, 32]. The extracted values of ideality factor and barrier height were 2.9 and 0.88 eV, respectively.

According with the thermionic emission theory, the ideality factor should be close to 1.01, a higher value of ideality factor indicates a secondary transport mechanism. Possible mechanisms may include interface dipoles or fabrication-induced defects at the interface [32]. Also, this higher value can be attributed to an insulating layer in the metal-semiconductor interface [30]. These extracted values are similar to those reported by other authors [30, 32].

In order to compare the effect of bending on the flexible devices, a flexible substrate was attached around a rigid plastic rod of 5 mm radius. The bent to a tensile radius of 5 mm is equivalent to a mechanical strain of ~0.5% [34]. **Figure 15** shows the bending effect of the flexible MIS devices. The electrical characteristics are very similar with and without bending, where the minor variations in current may be induced by an increase in tunneling under tensile strain. It is important to mention that these electrical characteristics are reversible after removal of the tensile strain.

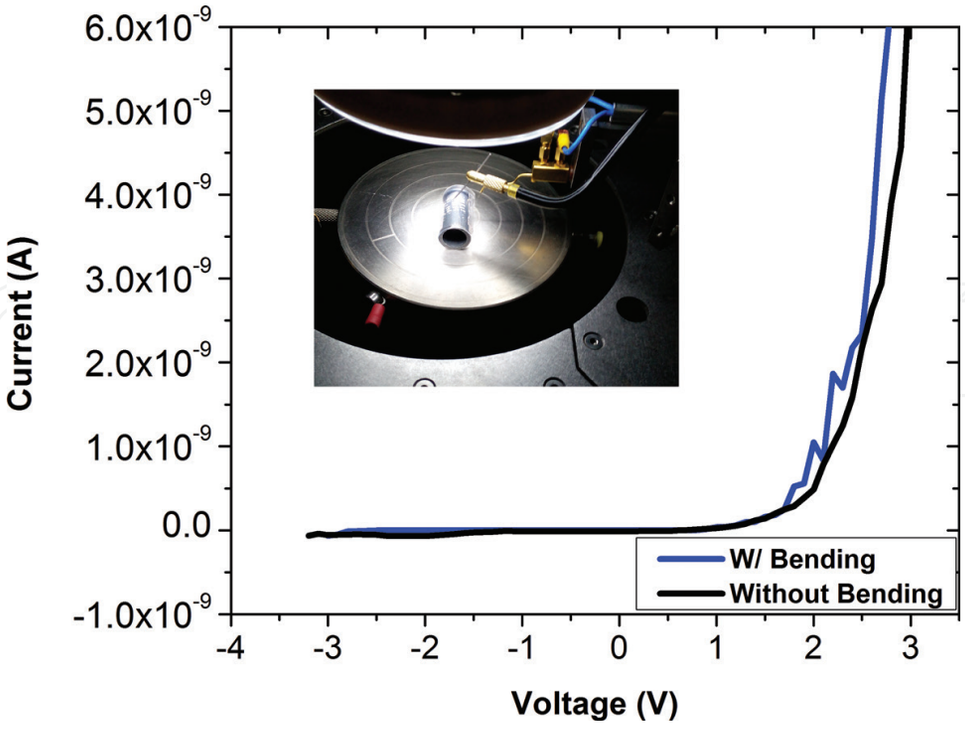

Figure 15. Electrical characteristics of the flexible devices with and without bending. Inset: Picture of the bent flexible MIS diodes.

These results show the potential of solution-processed AZO films to fabricate flexible semiconductor devices. The precursor solutions may be combined or replaced by new solutions in order to optimize the properties of the deposited thin films. The flexible MIS diodes were fabricated employing simple and low-cost solution process techniques under air ambient, using easily prepared precursor solutions.

3.3. Thin-film transistors

Although metal-oxide thin-film transistors (TFTs) fabricated by spray pyrolysis have already been demonstrated, the temperature of deposition to obtain high performance devices is still high to be compatible with most of the low-cost plastic substrates used in flexible and low-cost electronics. Then, it is necessary to reduce the temperature of deposition at values about 200°C or less in order to be a real alternative for low-cost applications. Moreover, yet, the role of the impurities and defects distribution in electronic properties of ZnO is still controversial, since they are highly dependent on the deposition technique and its conditions [10, 15, 35]. Therefore, the extraction of the density of states (DOS) within the gap of the ZnO is a great challenge and, typically, reflects contributions from the measurement techniques and interfaces from the TFT device [36–39].

Using this film as an active layer, inverted coplanar ZnO TFTs were fabricated. The transfer characteristics of the ZnO TFTs are presented in **Figure 16**. The electron field-effect mobility and threshold voltage were extracted from the square root of Ids versus Vgs, using Eq. (3) of the saturation regime [40].

http://dx.doi.org/10.5772/67548

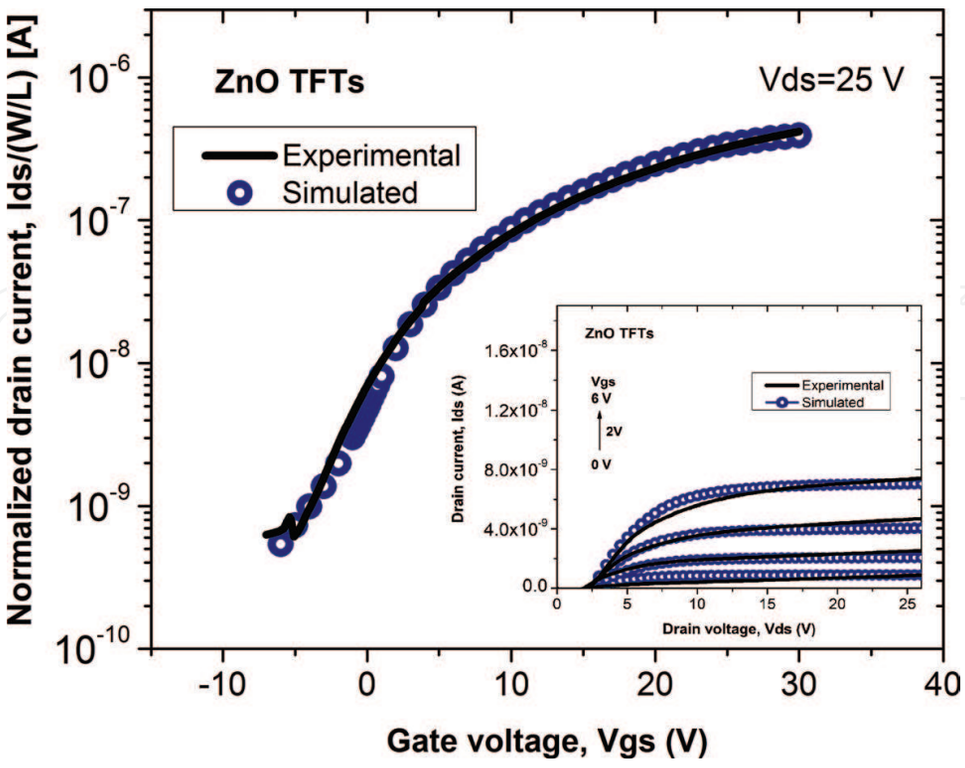

Figure 16. Experimental and simulated transfer characteristics of the ZnO thin-film transistors. Inset: Experimental and simulated output characteristics.

$$Ids = \mu FE \cdot C_{ox} (W/2L) (Vgs - V_T)^2 \quad (3)$$

where μ_{FE} is the electron field-effect mobility, C_{ox} is the capacitance per unit area of the gate insulator, W and L are the channel width and length, respectively, and V_T is the threshold voltage. The average value extracted was approximately 0.011 cm^2/Vs and 2.6 V for field-effect mobility and threshold voltage, respectively. The obtained results for ZnO TFTs with 50-nm-thick gate dielectric are better than those reported by Adamopoulos et al. [11]. They reported carrier mobilities from 0.003 to 0.001 cm^2/Vs and on/off-current ratios from 10^2 to 10^1 at deposition temperature of 200°C. Also, **Figure 16** shows the simulated transfer characteristic. The simulated data reproduces very well the experimental electrical characteristics of the device. The inset in **Figure 16** shows the experimental and simulated output characteristics. In order to reproduce the experimental electrical characteristics by physically based simulations, it is necessary to estimate approximately the density of states (DOS) within the gap of the ZnO film, commonly correlated to defects in the ZnO film. The typical DOS is composed of acceptor-like states (near the conduction band) given by the sum of tail states and deep states, and donor-like states (near the valence band) given by the sum of tail states and deep states [41].

The mathematical model of Silvaco simulator involves the Poisson's equation, the continuity equations and the transport equations to simulate any semiconductor device. In this mathematical model, using the TFT module, one can incorporate the DOS distribution g(E) proposed. The total charge caused by the presence of traps or defects is added into the right-hand side of Poisson's equation. Also, the recombination/generation rate in the carrier continuity

equations is modified by g(E). For accurate description of the model used in Silvaco simulator, please see Ref. [41]. The parameters used for the ZnO film and DOS were extracted from previous measurements (Section 2) and other Refs. [42, 43]. The DOS parameters were adjusted meanwhile the simulation fitted the experimental data.

The parameters used in the simulation for the DOS and ZnO film are listed in **Table 1**. As can be seen, the DOS obtained is higher than those previously reported by different authors [44, 45]. This can be due to more defects in the ZnO films originated by the incomplete precursor pyrolysis, corroborated by the presence of O—H complexes in the FTIR spectra and defects as the photoluminescence spectroscopy shows.

Parameter	Value	Description
N_C	5 x 10^{18} (cm^{-3})	Effective conduction band states
N_V	5 x 10^{18} (cm^{-3})	Effective valence band states
Eg	3.26 (eV)	Energy gap
Affinity	4.29 (eV)	Electron affinity
Permittivity	8.12	Dielectric constant
N_{TA}	1.95 x 10^{20} ($cm^{-3}eV^{-1}$)	Density of tail-acceptor states
N_{TD}	1.85 x 10^{20} ($cm^{-3}eV^{-1}$)	Density of tail-donor states
W_{TD}	0.385 (eV)	Decay energy of tail-donor
W_{TA}	0.105 (eV)	Decay energy of tail-acceptor
N_{GA}	1.2 x 10^{18} ($cm^{-3}eV^{-1}$)	Density of deep-acceptor states
E_{GA}	1 (eV)	Peak energy of deep-acceptor
W_{GA}	0.9 (eV)	Decay energy of deep-acceptor
N_d	9 × 10^{17} (cm^{-3})	Donor density
Rc	875 (Ωcm)	Contact resistance
μe	6 (cm^2/Vs)	Electron band mobility
μh	0.1 (cm^2/Vs)	Hole band mobility

Table 1. Main parameters used in the ZnO TFTs simulation.

4. Experimental section

For deposition of ZnO films, a home-made ultrasonic spray pyrolysis deposition system using air as carrier gas at flow rate of 467 sccm was used. The deposition system was adapted from an ultrasonic humidifier (Heaven Fresh). The precursor solution consists of zinc acetate (0.2 M) in methanol. The AZO films were deposited using a home-made ultrasonic spray pyrolysis deposition system adapted from an ultrasonic nebulizer (CITIZEN CUN-60) using air as the carrier gas, from 0.2 M precursor solution of zinc nitrate (Sigma-Aldrich) in distilled water, using aluminum nitrate (Sigma-Aldrich) as doping source at different molar concentration percentages with respect to zinc nitrate (M%). The samples were on a hotplate at 200°C during

deposition. The SOG/DI was obtained by spin-on glass (SOG700B Filmtronics) diluted 2:1 with deionized water (DI). The transparent electrodes were obtained using fluorine tin oxide (FTO) from 0.2 M precursor solution of tin tetrachloride pentahydrate in ethanol with ammonium fluoride diluted in deionized water prepared with Fluor/tin ratio of 0.52.

The optical transmittance of the thin films above corning glass was measured from 200 to 900 nm. The resistivity of the films was measured by four-point probe. The orientation of the films was obtained using an X-ray diffractometer (XRD) (Discover D8-Bruker axs) at 2θ range between 20° and 80° and 0.002° step. For the Photoluminescence spectroscopy, it was used as an exciting source, a laser of He-Cd with 325 nm line. The photoluminescence measurement was performed using a silicon PIN Thorlabs (DET-210) detector with a spectral response of 200–1100 nm. The IR absorption spectra of the films were measured with a "BRUCKER" FTIR spectrometer, Model Vertex-70. The IR spectrum was observed for wave numbers between 3500 and 400 cm^{-1}.

The flexible MIS diodes were fabricated above ITO-coated PET substrates (Sigma-Aldrich). First, the SOG/DI film was spin-coated at 5000 RPM for 30 sec and cured at 200°C for 1 h. Then, the AZO film was ultrasonic spray deposited at 200°C. As top electrodes, silver ink (AgIC Inks) was patterned. The contact area was 0.012 cm^2. The fabrication procedure of the inverted coplanar ZnO TFTs (bottom-contact bottom-gate) and transparent MIS capacitors can be found elsewhere [46, 47].

The electrical characteristics of the devices were measured using the Keithley-4200 Semiconductor Characterization System at room temperature and under dark conditions.

Acknowledgements

M. Dominguez wants to thank the financial support from NPTC-PRODEP by SEP-Mexico.

Author details

Miguel Dominguez*, Jose A. Luna-Lopez and Francisco J. Flores

*Address all correspondence to: madominguezj@gmail.com

Centro de Investigaciones en Dispositivos Semiconductores, Instituto de Ciencias, Benemerita Universidad Autonoma de Puebla (BUAP), Puebla, Mexico

References

[1] S. Fay, U. Kroll, C. Bucher, E. Vallat-Sauvain and A. Shah. Low pressure chemical vapour deposition of ZnO layers for thin-film solar cells: Temperature-induced morphological changes. Sol. Energy Mater. Sol. Cells. 2005;**86**:385.

[2] S.H. Mohamed and R. Drese. Structural and optical properties of direct current sputtered zinc aluminium oxides with a high Al concentration. Thin Solid Films. 2006;**513**:64.

[3] N. Bouhssira, S. Abed, E. Tomasella, J. Cellier, A. Mosbah, M. Aida and M. Jacquet. Influence of annealing temperature on the properties of ZnO thin films deposited by thermal evaporation. Appl. Surf. Sci. 2006;**252**:5594.

[4] J. Nishii, F.M. Hossain, A. Takagi, T. Aita, K. Saikusa, Y. Ohmaki, I. Ohkubo, S. Kishimoto, A. Ohtomo, T. Fukumura, F. Matsukura, Y. Ohno, H. Koinuma, H. Ohno and M. Kawasaki. High mobility thin film transistors with transparent ZnO channels. Jpn. J. Appl. Phys. 2003;**42**:L347.

[5] M. Olvera, H. Gomez and A. Maldonado. Doping, vacuum annealing, and thickness effect on the physical properties of zinc oxide films deposited by spray pyrolysis. Sol. Energy Mater. Sol. Cells. 2007;**91**:1449.

[6] P. Nunes, B. Fernandes, E. Fortunato, P. Vilarinho and R. Martins. Performances presented by zinc oxide thin films deposited by spray pyrolysis. Thin Solid Films. 1999;**337**:176.

[7] M. Dominguez, O. Obregon and J. Luna-Lopez. Study of stability of solution-processed dielectric film under electrical stress. J. Alloys Comp. 2016;**688**:893-896.

[8] A. Bashir, P. Wobkenberg, J. Smith, J. Ball, G. Adamopoulos, D. Bradley and T. Anthopoulos. High-performance zinc oxide transistors and circuits fabricated by spray pyrolysis in ambient atmosphere. Adv. Mater. 2009;**21**:2226-2231.

[9] G. Zhang, H. Wu, C. Chen, T. Wang, J. Yue and C. Liu. Transparent and flexible capacitors based on nanolaminate $Al_2O_3/TiO_2/Al_2O_3$. Nanoscale Res. Lett. 2015;**10**:76.

[10] D. Padilla, J. Vadillo and J. Laserna. Room temperature pulsed laser deposited ZnO thin films as photoluminescence gas sensors. Appl. Surf. Sci. 2012;**259**:806.

[11] G. Adamopoulos, A. Bashir, W. Gillin, S. Georgakopoulos, M. Shkunov, M. Baklar, N. Stingelin, D. Bradley and T. Anthopoulos. Structural and electrical characterization of ZnO films grown by spray pyrolysis and their application in thin- film transistors. Adv. Funct. Mater. 2011;**21**:525-531.

[12] R. Gayen, K. Sarkar, S. Hussain, R. Bhar and A. Pal. Zno films prepared by modified sol-gel technique. Indian J. Pure Appl. Phys. 2011;**49**:470-477.

[13] M.D. McCluskey, S.J. Jokela, K.K. Zhuravlev, P.J. Simpson and K.G. Lynn. Infrared spectroscopy of hydrogen in ZnO. Appl. Phys. Lett. 2002;**81**:3807.

[14] G. Shi, M. Stavola, S. Pearton, M. Thieme, E. Lavrov and J. Weber. Hydrogen local modes and shallow donors in ZnO. Phys. Rev. B. 2005;**72**:195211.

[15] S. Xiao, L. Zhao, Y. Liu and J. Lian. Nanocrystalline ZnO films prepared by pulsed laser deposition and their abnormal optical properties. Appl. Surf. Sci. 2013;**283**:781.

[16] S. Santra, P. Guha, S. Ali, P. Hiralal, H. Unalan, J. Covington, G. Amaratunga, W. Milne, J. Gardner and F. Udrea. ZnO nanowires grown on SOI CMOS substrate for ethanol sensing. Sensor Actuat. B Chem. 2010;**146**:559.

[17] D. Wang, H. Seo, C. Tin, M. Bozack, J. Williams, M. Park, N. Sathitsuksanoh, A. Cheng and Y. Tzeng. Effects of postgrowth annealing treatment on the photoluminescence of zinc oxide nanorods. J. Appl. Phys. 2006;**99**:113509.

[18] P. Nunes, A. Malik, B. Fernandes, E. Fortunato, P. Vilarinho and R. Martins. Influence of the doping and annealing atmosphere on zinc oxide thin films deposited by spray pyrolysis. Vacuum. 1999;**52**:45-49.

[19] P. Nunes, E. Fortunato and R. Martins. Influence of the annealing conditions on the properties of ZnO thin films. Inter. J. Inorg. Mater. 2001;**3**:1125-1128.

[20] J. Lee and B. Park. Characteristics of Al-doped ZnO thin films obtained by ultrasonic spray pyrolysis: Effects of Al doping and an annealing treatment. Mater. Sci. Eng. B. 2004;**106**:242-245.

[21] M. Jun, S. Park and J. Koh. Comparative studies of Al-doped ZnO and Ga-doped ZnO transparent conducting oxide thin films. Nanoscale Res. Lett. 2012;**7**:639.

[22] G. Sanon, R. Rup and A. Mansingh. Growth and characterization of tin oxide films prepared by chemical vapour deposition. Thin Solid Films. 1990;**190**:287.

[23] S. Kuo, W. Chen, F. Lai, C. Cheng, H. Kuo, S. Wang and W. Hsieh. Effects of doping concentration and annealing temperature on properties of highly-oriented Al-doped ZnO films. J Cryst Growth. 2006;**287**:78.

[24] D. Neamen. Semiconductor physics and devices. 3th ed. McGraw Hill, New York; 2003.

[25] Y. Yoo, J. Park, K. Lee, H. Lee, K. Song, S. Lee and H. Baik. Solution-processed high-k HfO_2 gate dielectric processed under softening temperature of polymer substrates. J. Mater. Chem. C. 2013;**1**:1651-1658.

[26] J. Park, Y. Yoo, K. Lee, W. Jang, J. Oh, S. Chae and H. Baik. Low-temperature, high-performance solution-processed thin-film transistors with peroxo-zirconium oxide dielectric. ACS Appl. Mater. Interf. 2013;**5**:410-417.

[27] Y. Son, J. Li and R. Peterson. In situ chemical modification of Schottky barrier in solution-processed zinc tin oxide diode. ACS Appl. Mater. Interf. 2016;**8**:23801.

[28] M. Green and J. Shewchun. Current multiplication in metal-insulator-semiconductor (mis) tunnel diodes. Solid State Electron. 1974;**17**:349.

[29] M. Hudait and S. Krupanidhi. Effects of thin oxide in metal-semiconductor and metal-insulator-semiconductor epi-GaAs Schottky diodes. Solid State Electron. 2000;**44**:1089.

[30] A. Tataroglu and S. Altındal. The analysis of the series resistance and interface states of MIS Schottky diodes at high temperatures using I–V characteristics. J. Alloys Comp. 2009;**484**:405.

[31] H. Jeong, H. Oh, S. Bang, H. Jeong, S. An, G. Han, H. Kim, S. Yun, K. Kim, J. Park, Y. Lee, G. Lerondel and M. Jeong. Metal–insulator–semiconductor diode consisting of two-dimensional nanomaterials. Nano Lett. 2016;**16**:1858.

[32] Ö. Güllü and A. Türüt. Electronic properties of Al/DNA/p-Si MIS diode: Application as temperature sensor. J. Alloys Comp. 2011;**509**:571.

[33] Zhe Chuan Feng. Handbook of Zinc Oxide and related materials Vol. 2. CRC Press, Florida; 2012.

[34] J. Jang, K. Cho, S. Lee and S. Kim. Transparent and flexible thin-film transistors with channel layers composed of sintered HgTe nanocrystals. Nanotechnology. 2008;**19**:015204.

[35] A. Janotti and C. Van de Walle. Native point defects in ZnO. Phys. Rev. B. 2007;**76**:165202.

[36] S. Baranovski. Charge transport in disordered solids with applications in electronics. 1st ed. Chichester: John Wiley & Sons Ltd; 2006.

[37] M. Dominguez, P. Rosales, A. Torres, F. Flores, J. Molina, M. Moreno, J. Luna and A. Orduña. Planarized Ambipolar a-SiGe:H thin-film transistors: Influence of the sequence of fabrication process. Solid State Electron. 2014;**99**:45-50.

[38] A. Nathan, S. Lee, S. Jeon and J. Robertson. Amorphous oxide semiconductor TFTs for displays and imaging. J. Display Technol. 2014;**10**:917-927.

[39] M. Dominguez, S. Alcantara and S. Soto. Physically-based simulation of zinc oxide thin-film transistors: Contact resistance contribution on density of states. Solid State Electron. 2016;**120**:41-46.

[40] M. Dominguez, P. Rosales and A. Torres. Performance improvement of low-temperature a-SiGe:H thin-film transistors. Solid State Electron. 2012;**76**:44-47.

[41] ATLAS User´s manual. Silvaco International, California; 2004.

[42] T. Fung, C. Chuang, C. Chen, K. Abe, R. Cottle, M. Townsend, H. Kumomi and J. Kanicki. Two-dimensional numerical simulation of radio frequency sputter amorphous In–Ga–Zn–O thin-film transistors. J. Appl. Phys. 2009;**106**:106:084511-1.

[43] F. Hossain, J. Nishii, S. Takagi, A. Ohtomo, T. Fukumura, H. Fujioka, H. Ohno, H. Koinuma and M. Kawasaki. Modeling and simulation of polycrystalline ZnO thin-film transistors. J. Appl. Phys. 2003;**94**:7768-7777.

[44] S. Bubel and M. Chabinyc. Model for determination of mid-gap states in amorphous metal oxides from thin film transistors. J. Appl. Phys. 2013;**113**:234507-1.

[45] S. Lee, D. Kim, E. Chong, Y. Jeon and D. Kim. Effect of channel thickness on density of states in amorphous InGaZnO thin film transistor. Appl. Phys. Lett. 2011;**98**:122105-1.

[46] M. Dominguez, F. Flores, A. Luna, J. Martinez, J. Luna-Lopez, S. Alcantara, P. Rosales, C. Reyes and A. Orduña. Impact of active layer thickness in thin-film transistors based on zinc oxide by ultrasonic spray pyrolysis. Solid State Electron. 2015;**109**:33-36.

[47] M. Dominguez and A. Orduna. Fully solution-processed zinc oxide MIS capacitors by ultrasonic spray pyrolysis in air ambient. J. Appl. Res. Technol. Forthcoming.